Redshift of few-cycle infrared pulses in the filamentation regime

2011 New J. Phys. 13 093005

(http://iopscience.iop.org/1367-2630/13/9/093005)

New Journal of Physics
The open-access journal for physics

Redshift of few-cycle infrared pulses in the filamentation regime

I Ahmad[1], L Bergé[2], Zs Major[1,3], F Krausz[1,3], S Karsch[1,3] and S A Trushin[1,4]

[1] Max-Planck-Institut für Quantenoptik (MPQ), Hans-Kopfermann-Strasse 1, D-85748 Garching, Germany
[2] CEA-DAM, DIF, F-91297 Arpajon, France
[3] Ludwig-Maximilians-Universität München, Am Coulombwall 1, D-85748 Garching, Germany
E-mail: sergei.trushin@mpq.mpg.de

New Journal of Physics **13** (2011) 093005 (12pp)
Received 28 February 2011
Published 1 September 2011
Online at http://www.njp.org/
doi:10.1088/1367-2630/13/9/093005

Abstract. By focusing infrared (IR) pulses of low energy (∼0.4 mJ) into an argon cell at a pressure of a few bars, a supercontinuum is generated with a long-wavelength tail that can exceed 1500 nm for initial pulse durations of ∼5 fs in the single-filamentation regime. Numerical calculations simulating the propagation of single- or few-cycle IR pulses show that this red-shift is enhanced by a sharp leading edge appearing in the pulse temporal profile, as the pulse undergoes break-up due to the interplay between Kerr self-focusing, strong dispersion and plasma generation.

[4] Author to whom any correspondence should be addressed.

Contents

1. Introduction

In nonlinear optical media, self-phase modulation (SPM) is induced by the change in refractive index due to the optical Kerr effect $\Delta n_{\rm kerr} = n_2\, I(t)$, proportional to the time-dependent pulse intensity $I(t)$ and material nonlinear index n_2. The SPM modulates the phase of ultrashort laser pulses, introducing new frequencies with a temporal chirp, and is able to generate a broad supercontinuum. Combined with group-velocity dispersion and optimized with chirped mirror compressors, SPM can be exploited to produce pulses with durations down to a few optical cycles in, e.g., gas-filled hollow waveguides at appropriate pressures [1–3]. High-power pulses propagating in full three-dimensional (3D) media develop other interesting features, such as 'filamentation'. Supercontinuum generation during the nonlinear filamentation of femtosecond pulses in air and other gases has been extensively studied [4–9]. Due to the spatial profile of intensity $I(t, r)$ and at high enough power, the same term $n_2 I(t)$ causing SPM gives rise to a focusing lens effect, named self-focusing. When the laser power is above the critical value for self-focusing $P_{\rm cr} \approx \lambda_0^2/(2\pi n_2)$ at a given wavelength λ_0, the beam can develop a collapse dynamics. This singular process is halted, however, by a defocusing effect produced by the electron plasma, which is created by ionization of gas atoms at such high intensities. This plasma is usually visible as a luminescent channel.

Within a simple approximation described in [10, 11] the supercontinuum frequency spread was proposed to be proportional to the inverse of the pulse duration, meaning the shorter the pulse, the broader the generated spectrum. This simple model predicts a frequency-symmetric broadening. However, by self-steepening [4] the slope of the rear edge of the pulse is increased abruptly, which gives rise to a very large blueshift. The blue part of such supercontinuum generation has been extensively studied for ultrashort 800 nm pulses with mJ energy. The spectral broadening in the single-filamentation regime in Ar or air results in a supercontinuum extending down to 200 nm in the ultraviolet [12–15], which is essential for single-cycle nonlinear optics, ultrafast spectroscopy [1, 16] and attosecond physics [17]. While most studies have been devoted to the wavelength region below 1100 nm, supercontinuum generation by filamentation into the infrared (IR) has received limited attention to date. It has been demonstrated that by focusing terawatt laser beams in air under conditions of multiple filamentation, the supercontinuum can be extended to the mid- and far-IR [18–20]. It was inferred that the dominant mechanism for such long IR tail generation is four-wave mixing (4WM) between the pump pulse and its blue-shifted conical emission [19, 20]. The extension

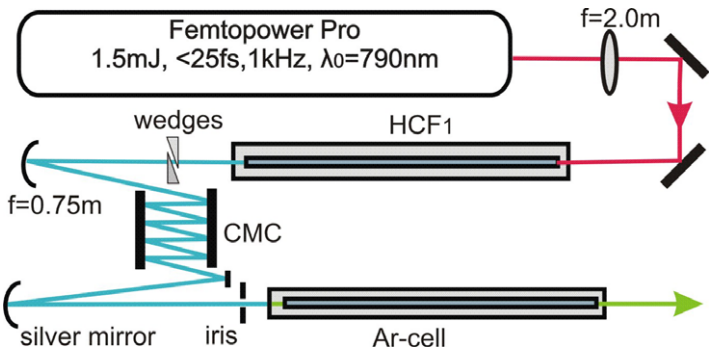

Figure 1. Schematic layout of the experimental setup. 'CMC' indicates a chirped mirror compressor.

of supercontinua into the near-IR (NIR) domain by single filamentation of μJ-scale-energy femtosecond pulses at different pump wavelengths in transparent solids was examined recently in [21].

In this paper, we present our findings on the long-wavelength part of the supercontinuum produced by filamentation of few-cycle mJ-scale pulses near 800 nm in Ar. This investigation was motivated by the need for high-energy, broadband pulses in the NIR domain derived from a Ti:sapphire source for seeding novel optical parametric amplifiers [22]. In addition, our experimental and theoretical study sheds light on the underlying mechanism of the NIR supercontinuum generation by filamentation. We show, for the first time, that this spectral domain can be extended beyond 1500 nm under single-filament conditions. Preliminary experimental results were communicated briefly in [22]. The spectral dynamics are mostly supported by direct numerical simulations, which, in addition to the classical optical Kerr-induced SPM broadening, display the link between the build-up of NIR wavelengths and an enhancement of the leading edge of the pulse.

2. Experimental method and results

A schematic layout of the experimental setup is shown in figure 1. The few-cycle light pulses are generated by post-compression of the spectrally broadened output of a hollow-core fibre (HCF). Here, 1.5 mJ, sub-25 fs pulses centred near 790 nm from a commercial Femtopower laser source (Femtolasers GmbH) are focused by an $f = 2$ m lens into a 300 μm inner diameter and 1 m long HCF filled with Ne. We observed a throughput efficiency $>50\%$. The output is then collimated by a 0.75 m focal length silver-coated mirror and compressed using a negatively chirped mirror compressor. These mirrors provide a flat group delay dispersion (GDD) of -40 fs^2 per reflection in a broad spectral range of 550–1000 nm. We use a pair of wedges in order to fine-tune the dispersion of the pulse for compression. The pulses are subsequently focused through a silver-coated mirror into a 158 cm long argon cell (Ar cell), where a filament forms. The resulting broadband supercontinuum at the Ar-cell output is measured using the AvaSpec-3648 and AvaSpec-NIR256-1.7 (Avantes) spectrometers. Spectra were recorded at 1 m beyond the cell after an iris has been used to limit the beam to its central spot and to cut its conical emission. This spot was then coupled into the entrance of the spectrometer.

This paper is dedicated to the spectral broadening of the IR tail in filaments depending on various parameters such as the input pulse duration, energy and gas pressure. Although our

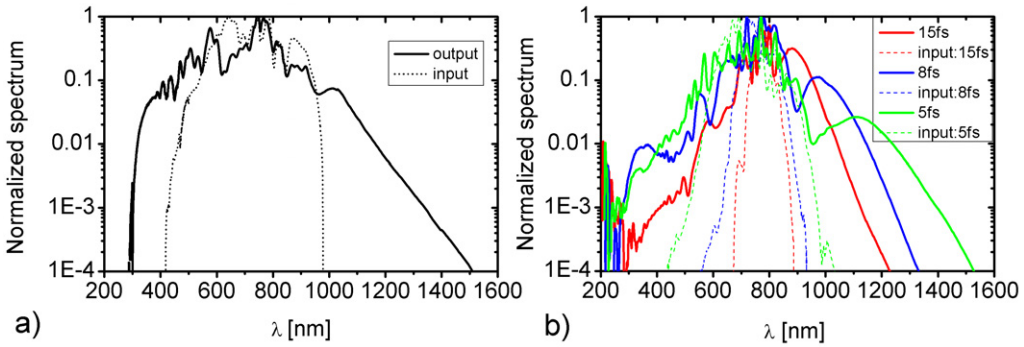

Figure 2. (a) Normalized intensity spectrum of the supercontinuum generated by filamentation in Ar by a 4.2 fs pulse at 0.8 bar pressure. (b) Normalized intensity spectra of the supercontinuum generated by filamentation in Ar by 15 fs (red curves), 8 fs (blue curves) and 5 fs (green curves) nearly Gaussian pulses at 2 bar pressure. The dotted lines in respective colours represent the spectra of the input pulses.

experimental results were achieved under different circumstances, i.e. the focusing conditions and pressure values may differ from one experiment to another, our numerical simulations qualitatively reproduce the observed propagation dynamics for beam and medium parameters close to the experimental conditions (see section 3).

2.1. Pulse width dependence

The spectral broadening in the HCF strongly depends on its local pressure and therefore the resulting compressed pulse duration also varies with pressure. This principle was used to produce pulses of 4.2, 5, 8 and 15 fs full-width at half-maximum (FWHM) duration by compression of the HCF output spectra at 2.4, 2.0, 0.8 and 0.4 bar of Ne, respectively. The FWHM pulse durations were measured using an interferometric autocorrelator (Femtolasers GmbH), which can resolve pulse durations down to 4 fs. Special care was taken to select the input pulse profile with minimum duration and remaining close to its transform limit. The maximum deviation from the transform limit was 23% of the FWHM pulse duration. For example, although the spectrum of our shortest pulse centred at ∼720 nm (see the dotted curve in figure 2(a)) supports a transform limited pulse duration of 3.4 fs, the measured FWHM pulse duration was 4.2 fs. Such pulses allow us to investigate the propagation dynamics close to the single-cycle regime. For these shortest pulses the spectral broadening experiments were carried out by focusing the pulses with an input beam waist, i.e. $1/e^2$ radius of the intensity profile, of 2.2 mm by a silver mirror of 150 cm focal length into the Ar cell maintained at 0.8 bar pressure. The available pulse energy of 450 μJ after the chirped mirror compressor was limited to 400 μJ to avoid multiple filamentation and the pulses initially exhibited an almost Gaussian profile in space and close to transform-limited in time. The generated spectrum is presented in figure 2(a), showing evidence of a supercontinuum spanning more than two octaves and of a significant build-up of long wavelengths.

The systematic dependence of the spectral broadening on different input pulse durations is presented in figure 2(b). All input pulses with the measured pulse durations of 5, 8 and 15 fs

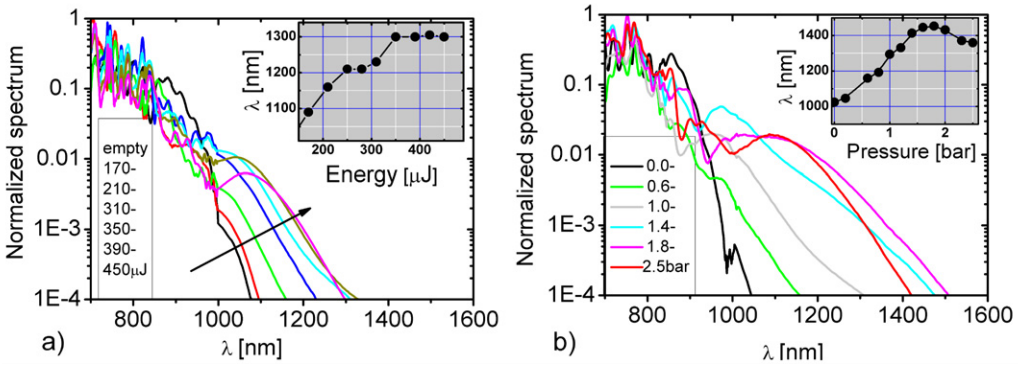

Figure 3. (a) Dependence of the long-wavelength part of the supercontinuum on the energy of 5 fs incident pulses at a fixed Ar pressure of 1 bar. (b) Dependence of the long-wavelength part of the supercontinuum on Ar pressure for 5 fs pulses at a fixed energy of 400 μJ. Insets show the cut-off wavelengths of the NIR part of the spectra at the 10^{-4} level of the normalized peak values.

remained within 10% of their transform limit. The shape of the nearly transform-limited input pulses for our input spectra remained practically Gaussian for intensities above 10^{-2} of the normalized temporal profile. In this case, the central wavelength was about 780 nm and the beam waist at the position of the focusing mirror was 1.8 mm. These pulses were focused with an $f = 200$ cm silver mirror into the Ar cell, where a single light filament was formed. Figure 2(b) depicts the spectra of the input pulses (dashed curves) as well as the resulting supercontinua at the output of the Ar cell (solid curves) for a fixed gas pressure of 2 bar and pulse energy of 400 μJ. It is clear that the NIR tail of the supercontinuum increases with decreasing pulse duration. We can define a long-wavelength cut-off, where the spectral intensity drops to the 10^{-4} level of the normalized peak value. This cut-off moves from 1230 to $\sim$1500 nm when the FWHM pulse duration is shortened from 15 to 5 fs. At higher spectral intensity levels, a maximum (hump) in the spectrum is seen located around $900 \leqslant \lambda \leqslant 1200$ nm, which shifts to longer wavelengths as the pulse duration decreases. The broadband supercontinuum obtained with the 5 fs pulse supports sub-cycle 1.7 fs pulses at 700 nm central wavelength.

2.2. Pulse energy dependence

In this part of the experiment, we used a 5 fs pulse with different energies at a fixed Ar pressure of 1 bar. The pulses with a beam waist of 1.8 mm were focused into the Ar cell using a 200 cm focal length silver mirror. The pulse energy at the input of the Ar cell was varied by placing an iris into the incident beam. The NIR parts of the supercontinua are shown in figure 3(a). The inset depicts the cut-off wavelengths of this spectral domain at the 10^{-4} level of the normalized peak values. The cut-off wavelengths increase with the pulse energy at fixed pulse duration and pressure. They shift from 1100 to 1300 nm when the energy is varied from 170 to 450 μJ, respectively. The energy dependence of the cut-off wavelengths levels off around 400 μJ input energy, indicating that no further spectral broadening towards the NIR domain occurs. Since above this input energy multiple filamentation sets in, we can infer that the maximum NIR broadening for a single filament propagating over meter-range distances at a given pressure is obtained just below this threshold.

2.3. Pressure dependence

Here the 5 fs pulses with a fixed energy of 400 μJ are used to study the effect of pressure variation on the spectra generated by filamentation. The pulses with a beam waist of 1.8 mm were focused using an $f = 200$ cm silver mirror into the Ar cell. The argon pressure was changed from zero to 2.5 bar. Figure 3(b) depicts the NIR tail of the resulting supercontinua. The inset shows the cut-off wavelengths of the NIR part of the spectra at the 10^{-4} levels of the normalized peak values. While increasing pressure, we observe a nearly linear increase of the cut-off wavelength, which reaches a maximum and then decreases at an even higher pressure. A maximum occurs at a pressure of 1.8 bar, around which the cut-off wavelength extends to $\sim$1500 nm.

3. Theoretical results and discussion

To understand the origin of the above redshifts, we performed numerical simulations using the forward Maxwell equation as employed in, e.g., [6, 23]. This model describes the forward high-frequency electric field of ultrashort optical pulses being linearly polarized and subject to diffraction, full chromatic dispersion, Kerr self-focusing, plasma generation and self-steepening. Plasma generation involves the Perelomov–Popov–Terent'ev ionization rate [24] applied to argon, whose linear dispersion curve is that computed by Dalgarno and Kingston [25] and the Kerr index n_2 follows Shelton's evaluations [26]. This propagation model describes third-order harmonic generation produced by the nonlinear (cubic) polarization vector. For symmetry reasons, we limit our theoretical analysis to radially symmetric optical structures, except in figure 5 below. With this theoretical study we gain insight into the physical mechanisms underlying the filamentation process for the extreme case of near single-cycle input pulses, which has not been explored yet.

To start with, we investigated a transform-limited pulse with a Gaussian spectrum and FWHM duration of 3.4 fs, which corresponds to the shortest pulse duration supported by the broadest spectrum in our experiments. Figure 4 details the characteristic dynamics of this pulse at moderate power, i.e. $15P_{\rm cr}$ ($P_{\rm cr} = 5.67$ GW, $E_{\rm in} = 310\,\mu$J), and operating at 720 nm central wavelength. Following the setup related to figure 2(a), the pulse at $z = 0$ has an input beam waist of 2.2 mm and is focused by a lens of focal length $f = 150$ cm. As shown in figure 4(a), the pulse self-focuses at $z = z_{\rm c} \approx 1.25$ m due to the optical Kerr effect. It generates a tenuous plasma of maximum density limited to 1.5×10^{17} cm^{-3}, leading to filament self-channeling over $\sim$20 cm (z denotes the longitudinal propagation variable) with a mean clamping intensity of $\sim$100 TW cm^{-2}. The inset details the intensity distribution of the pulse in the t–z-plane along the self-channeling range. Figure 4(b) contains the temporal profiles at different z-positions along the same range. The time variable refers to a retarded time expressed in the frame moving with the linear group velocity of the pulse [6]. Slight temporal oscillations are caused by interferences between the pump and the third harmonic. Figure 4(c) shows the corresponding spectra, averaged over the simulation box. Starting with a near-one-cycle purely Gaussian pulse ($\tau_{\rm o.c.} = \lambda_0/c = 2.4$ fs), the pulse spectrum is initially already broad, with a net asymmetry at long wavelengths compared with figure 2(a), and it will be broadened even more due to the following processes. Owing to the dispersion, the pulse significantly lengthens in time before the nonlinear focus $z_{\rm c}$. Beyond this point, pulse break-up occurs while self-steepening favours a shock profile at the trailing edge of the pulse ($t > 0$) along one focusing–defocusing sequence.

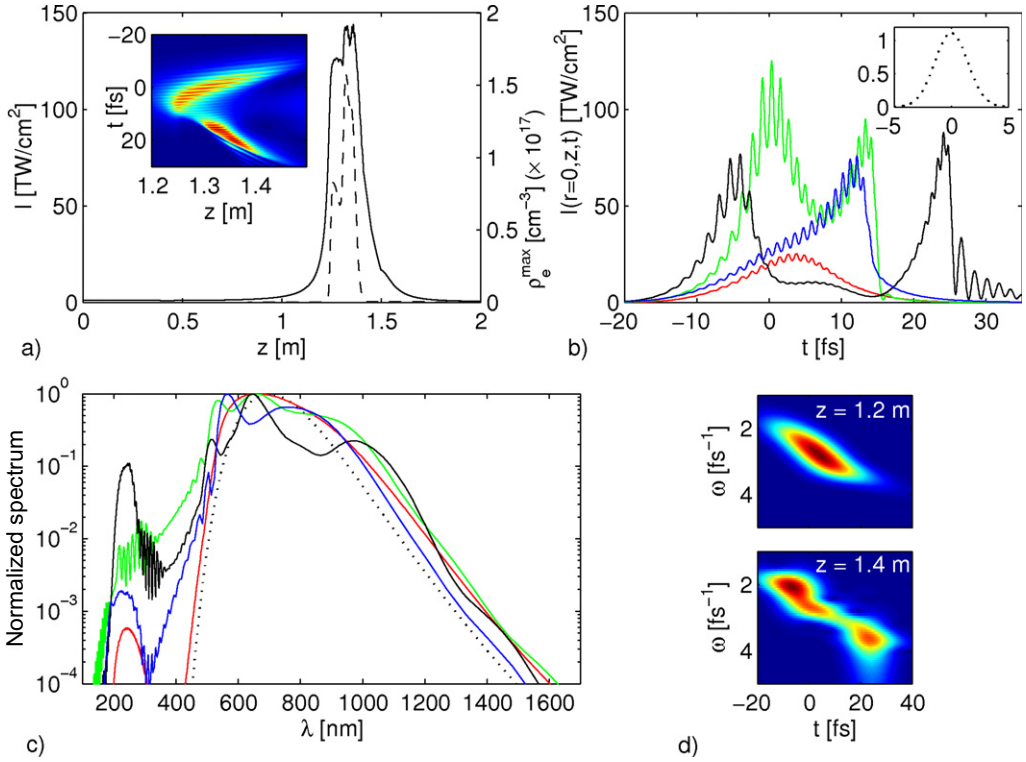

Figure 4. (a) Peak intensity (solid curve, left-hand side axis) and plasma density (dashed curve, right-hand side axis) developed in the filamentation regime by a 3.4 fs Gaussian pulse at 720 nm with $15\,P_{\mathrm{cr}}$ in converging geometry ($f = 150$ cm) and in Ar at 0.8 bar pressure. The inset zooms the temporal dynamics between $z = 1.2$ m and $z = 1.5$ m. (b) Temporal profiles at the propagation distances $z = 1.2$ m (red curve), $z = 1.3$ m (green curve) and $z = 1.4$ m (black curve). The dotted curve in the inset specifies the pulse profile at $z = 0$. The time variable corresponds to a retarded time $t \rightarrow t + z/v_{\mathrm{g}}$ expressed in the frame moving with the group velocity v_{g} and keeping the pulse centre at zero delay. The blue curve shows the same pulse with reduced power, i.e. $5\,P_{\mathrm{cr}}$ only, at $z = 1.5$ m. (c) Corresponding normalized intensity spectra averaged in the simulation box at the same distances; the dotted curve refers to the input spectrum. (d) XFROG traces for the 15 P_{cr} pulse at specific distances.

Besides this shock dynamics responsible for the creation of blue shoulders in the spectra [13], the major feature is the occurrence of the focusing leading edge, i.e. sharp temporal gradients emerge in the front pulse ($t < 0$) (figure 4(b)).

Since frequency variations are directly linked to the temporal gradient of the nonlinear phase describing the interplay between Kerr self-focusing and plasma generation, a strong redshift marks the spectra driven by the steepest components of the front pulse [27]. In gas-based self-compression experiments mediated by filamentation, the pulses often attain few-cycle durations by enhancing their rear part to the detriment of the front one [28]. In the present context, we see the reverse route. A single-cycle pulse undergoes strong dispersion in time and self-focusing in space. The former starts to spread out the pulse in time, but contributes

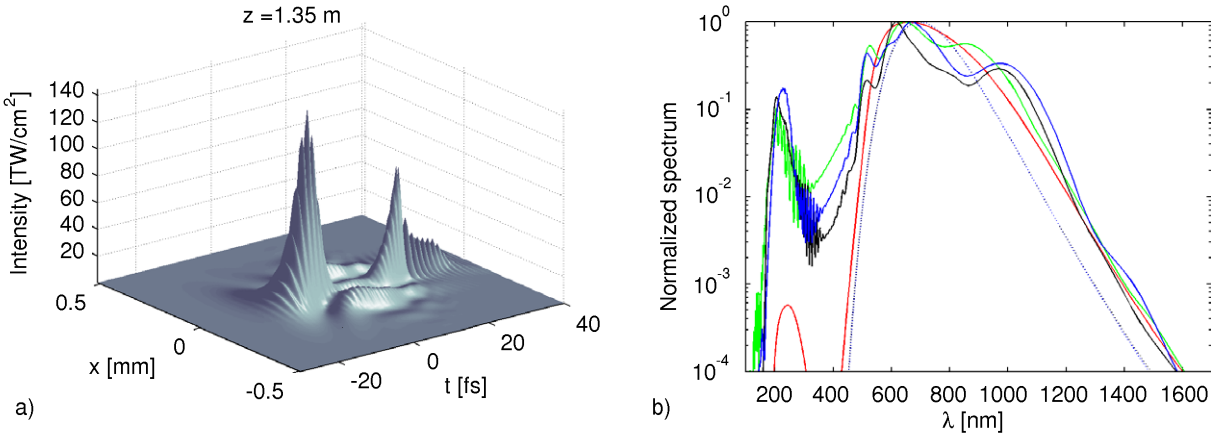

Figure 5. (a) Maximal intensity in the plane (x, t) along the line $y = 0$ at $z = 1.35$ m for the same Gaussian pulse with 15 P_{cr} as in figure 4, but simulated in full 3D geometry. (b) Normalized averaged intensity spectra with the same color coding as in figure 4(c). The blue solid curve shows the redshift undergone in the filamentation regime by a 3.4 fs, 720 nm input pulse having a fourth-order super-Gaussian profile in space and a Gaussian profile in time perturbed by a 5% amplitude random noise. Dotted curves represent the spectrum at $z = 0$.

to promote pulse splitting through normal group-velocity dispersion near z_c [6], whereas the latter triggers plasma defocusing that also breaks up the pulse. At high enough powers, plasma generation and dispersion thus both favour pulse break-up. The Gaussian pulse is lengthened up to 14 fs at $z = 1.2$ m due to linear dispersion and then up to 45 fs due to plasma-induced pulse break-up. The resulting spectrum is broadened to almost three octaves (from 200 to 1600 nm) and the cut-off wavelength at the 10^{-4} level is redshifted by about 150 nm compared with the initial spectrum. To check our statement, we performed simulations discarding harmonic generation, self-steepening or dispersion. Only when dispersion was cancelled, the propagation pattern drastically changed, i.e. the nonlinear focus noticeably moved to shorter distances while the pulse tried to preserve its initial temporal profile at higher clamping intensity (not shown). Therefore, at $z = 1.2$ m, SPM and dispersion are mainly responsible for the first redshift (see the red curve in figure 4(c)). Note that as the blue-visible bandwidth is enhanced by self-steepening, four-wave mixing ($\omega_{4WM} = 2\omega_0 - \omega_s$) between the pump frequency (ω_0) and seeded high frequencies (ω_s) may also contribute to the production of IR components, provided that $\omega_s < 2\omega_0$. However, creating wavelengths above 1500 nm requires the condition of exciting the spectral interval $360 \leqslant \lambda_s \leqslant 474$ nm ($3.88 \leqslant \omega_s \leqslant 5.24$ fs^{-1}), which seems barely fulfilled at this stage. At later distances ($z \geqslant 1.3$ m), plasma-induced pulse break-up promotes sharp gradients in the front zone and 4WM can be more efficient. A second stage develops, characterized by the occurrence of a 'red shoulder' (or 'red hump'), centred around 1100 nm and visible between the levels 10^{-2} and 10^{-1} in both the experiments (figures 2 and 3) and the numerical data (figures 4 and 5).

This spectral evolution definitively requires sharp leading edges in the pulse profile. To underline the importance of the front pulse shape, we also plotted the temporal profile of the same pulse simulated with lower power ($5P_{cr}$). At clamping intensity, this pulse only steepens its trailing edge (see the blue curve in figure 4(b)), while the plasma density remains limited to a few 10^{15} cm^{-3}. In that case, the generated supercontinuum covers the previous interval of

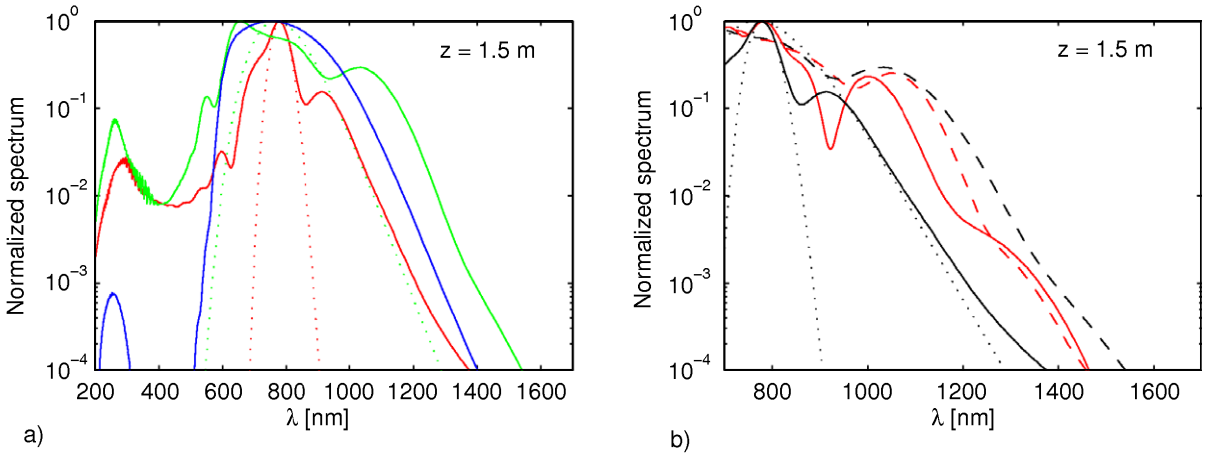

Figure 6. (a) Normalized intensity spectra for 780 nm Gaussian pulses with a beam waist of 1.8 mm, focused by an $f = 200$ cm lens in a 2 m long Ar gas cell at 1 bar pressure with $14.1\,P_{cr}$ (400 μJ energy). FWHM pulse duration is either 5 fs (green curve) or 15 fs (red curve). The blue curve refers to the 5 fs pulse with half-energy ($7.05\,P_{cr}$). Snapshot distance is $z = 1.5$ m along the self-channeling range. The dotted curves correspond to spectra at $z = 0$. (b) The same pulses with 400 μJ energy at different pressures: 2 bar (red dashed curve) and 1 bar (black dashed curve) for the 5 fs pulse; 2 bar (red solid curve) and 1 bar (black solid curve) for the 15 fs pulse.

high frequencies seeded for 4WM better (see the blue curve in figure 4(c)). Nonetheless, the redshift remains limited to the broadening primarily caused by SPM, compare, e.g., with the red curve in figure 4(c). These behaviours indicate that the 'red hump' develops from the dynamical competition between all nonlinearities and dispersion yielding a prominent leading edge at high enough peak intensities. In figure 4(d), we show a couple of cross-correlation frequency-resolved optical gating (XFROG) traces for the $15\,P_{cr}$ pulse at the distances $z = 1.2$ and 1.4 m. These traces confirm that the growth of the leading edge at negative times is associated with the enhancement of IR wavelengths, while the steepening of the trailing edge at positive times is associated with an additional build-up of blue wavelengths in the spectrum. They also indicate that, despite pulse splitting, the group delay remains a single-valued function of the frequency.

To confirm the generic nature of our findings, we simulated the same Gaussian pulse by using a full 3D unidirectional propagation model exploiting a quasistatic tunnel ionization rate [29]. An analogous dynamic was observed. As seen from figure 5(a), the spatiotemporal (x, t) intensity distribution of the pulse in the longitudinal interval $1.3 < z < 1.4$ m reproduces the sharpening of the front pulse and confirms that multiple filamentation, i.e. the amplification of out-of-axis optical components, does not take place at incident peak powers limited to $15\,P_{cr}$. In figure 5(b), the normalized intensity spectra faithfully reproduce those shown in figure 4(c). The solid blue curves represent the redshift promoted by an input pulse having a fourth-order super-Gaussian profile in space, as it can exit from a variable aperture used to select the beam energy, and a Gaussian amplitude in time perturbed by a 5% random noise. Apart from secondary ring formation that precedes the nonlinear focus (not shown), such super-Gaussian pulses develop similar dynamical features in the filamentation regime, which leads to comparable, and thus generic, spectral redshifts.

In connection with figures 2(b) and 3, we further analysed variations of the red part of the spectra by simulating 780 nm Gaussian pulses with a 1.8 mm waist and having different FWHM durations and input energies. These pulses are focused by an $f = 200$ cm lens and produce filaments inside a 2 m long Ar cell at various pressures. Depending on the laser parameters and the local pressure, the beam self-focuses near $z = 1.2$–1.3 m and self-channels over several tens of cm beyond. In figure 6, we show the averaged intensity spectra computed at the distance $z = 1.5$ m, which represents the half-distance of the self-guiding range among all investigated configurations. At 1 bar pressure, figure 6(a) shows the changes in the redshifted spectrum when the pulse duration is increased from 5 fs (green curve) to 15 fs (red curve) with 400 μJ energy. The IR cut-off at the 10^{-4} level decreases by about 150 nm. The blue curve refers to the 5 fs pulse whose energy has been divided by a factor 2, which reduces the redshift by about 100 nm at the same level. A comparison with figures 2(b) and 3(a) shows that there is close agreement between our experimental and theoretical findings. Figure 6(b) shows variations of the redshifted zone with the local pressure obtained from numerical computations. We observe a broadening of the IR tail for sub-two-cycle pulses (5 fs) when the pressure is decreased. This follows from the delicate variations in the ratio of the nonlinear refractive index change to the effective pulse duration, both of which increase with pressure along propagation. Discrepancies between simulations and experiment (see figure 3(b)) can be attributed to the higher-order dispersion that was not fully compensated for in the experimental setup and therefore yielded a different 5 fs pulse profile and shorter filament lengths. In contrast, 15 fs pulses are less sensitive to dispersion, thus their spectral evolution does reproduce an increase of the redshift with pressure. For the 5 fs pulse, the simulations predict a comparable redshift cut-off at 2 bar pressure, e.g. about 1460 nm at the 10^{-4} level. This value agrees reasonably well with the experimental data reported in figure 3(b).

Finally, we would like to emphasize that in all our numerical computations, the spectral phase was found to be a single-valued function of the frequency over the whole spectrum. Hence, the previous pulses are expected to be compressible down to a transform-limited pulse duration close to 2 fs by appropriate dispersion management.

4. Conclusion

In summary, we have demonstrated the generic occurrence of significant redshifts characterizing infrared few-cycle pulses that undergo single filamentation in a pressurized argon cell. Direct numerical simulations revealed that, for near-single-cycle pulses and at high enough powers, this redshift first develops in a classical SPM broadening stage, followed by a second enhancement induced by sharp leading edges that mark the temporal pulse profile. Initiated by plasma defocusing and strong dispersion, this two-peaked profile preserves a focused front over a long distance, which is associated with the largest redshift in the spectrum. Our numerical calculations also reproduced most of the trends of the experimental spectral broadenings as a function of pulse duration, input energy and pressure. These findings support the validity of our model for sub-two-cycle pulses, a regime that should be routinely accessible in the near future. Furthermore, our theoretical results suggest that the shortest pulses developing the broadest spectra are compressible to about 2 fs transform-limited pulse duration by employing appropriate post-compression techniques.

Acknowledgments

This work was funded by the Max-Planck Society through the PFS grant. Financial support from the Extreme Light Infrastructure and the DFG Cluster of Excellence, Munich Centre for Advanced Photonics, is also acknowledged. IA is grateful for support through the joint doctoral fellowship of the Deutscher Akademischer Austausch Dienst (DAAD) and the Higher Education Commission (HEC) with grant number HEC-DAAD-2006/11586.

References

[1] Brabec T and Krausz F 2000 Intense few-cycle laser fields: frontiers of nonlinear optics *Rev. Mod. Phys.* **72** 545
[2] Nisoli M, De Silvestri S and Svelto O 1996 Generation of high energy 10 fs pulses by a new pulse compression technique *Appl. Phys. Lett.* **68** 2793
[3] Nisoli M, De Silvestri S, Svelto O, Szipöcs R, Ferencz K, Spielmann Ch, Sartania S and Krausz F 1997 Compression of high-energy laser pulses below 5 fs *Opt. Lett.* **22** 522
[4] Chin S L, Hosseini S A, Liu W, Luo Q, Théberge F, Aközbek N, Becker A, Kandidov V P, Kosareva O G and Schroeder H 2005 The propagation of powerful femtosecond laser pulses in optical media: physics, applications, and new challenges *Can. J. Phys.* **83** 863
[5] Couairon A and Mysyrowicz A 2007 Femtosecond filamentation in transparent media *Phys. Rep.* **441** 47
[6] Bergé L, Skupin S, Nuter R, Kasparian J and Wolf J-P 2007 Ultrashort filaments of light in weakly ionized, optically transparent media *Rep. Prog. Phys.* **70** 1633
[7] Kasparian J and Wolf J-P 2008 Physics and applications of atmospheric nonlinear optics and filamentation *Opt. Express* **16** 466
[8] Hauri C P, Kornelis W, Helbing F W, Heinrich A, Couairon A, Mysyrowicz A, Biegert J and Keller U 2004 Generation of intense, carrier-envelope phase-locked few-cycle laser pulses through filamentation *Appl. Phys.* B **79** 673
[9] Stibenz G, Zhavoronkov N and Steimeyer G 2006 Self-compression of millijoule pulses to 7.8 fs duration in a white-light filament *Opt. Lett.* **31** 274
[10] Manassah J T 1989 *The Supercontinuum Laser Source* ed R R Alfano (New York: Springer) p 184
[11] Kosma K, Trushin S A, Fuss W and Schmid W E 2008 Characterization of the supercontinuum radiation generated by self-focusing of few-cycle 800 nm pulses in argon *J. Mod. Opt.* **55** 2141
[12] Trushin S A, Panja S, Kosma K, Schmid W E and Fuss W 2005 Supercontinuum extending from >1000 to 250 nm, generated by focusing 10-fs laser pulses at 805 nm into Ar *Appl. Phys.* B **80** 399
[13] Aközbek N *et al* 2006 Extending supercontinuum spectrum down to 200 nm by self-phase modulation of few-cycle 800-nm pulses in argon *New J. Phys.* **8** 177
[14] Skupin S and Bergé L 2007 Supercontinuum generation of ultrashort laser pulses in air at different central wavelengths *Opt. Commun.* **280** 173
[15] Goulielmakis E, Koehler S, Reiter B, Schultze M, Verhoef A J, Serebryannikov E E, Zheltikov A M and Krausz F 2008 Ultrabroadband, coherent light source based on self-channeling of few-cycle pulses in helium *Opt. Lett.* **33** 1407
[16] Goulielmakis E *et al* 2008 Single-cycle nonlinear optics *Science* **320** 1614
[17] Krausz F and Ivanov M 2009 Attosecond physics *Rev. Mod. Phys.* **81** 163
[18] Kasparian J *et al* 2003 White-light filaments for atmospheric analysis *Science* **301** 61
[19] Théberge F, Châteauneuf M, Ross V, Mathieu P and Dubois J 2008 Ultrabroadband conical emission generated from the ultraviolet up to the far-infrared during the optical filamentation in air *Opt. Lett.* **33** 2515
[20] Théberge F, Châteauneuf M, Roy G, Mathieu P and Dubois J 2010 Generation of tunable and broadband far-infrared laser pulses during two-color filamentation *Phys. Rev.* A **81** 033821

[21] Bradler M, Baum P and Riedle E 2009 Femtosecond continuum generation in bulk laser host materials with sub-μJ pump pulses *Appl. Phys.* B **97** 561
[22] Ahmad I *et al* 2009 Frontend light source for short-pulse pumped OPCPA system *Appl. Phys.* B **97** 529
[23] Wang Z, Liu J, Li R and Xu Z 2009 Supercontinuum generation and pulse compression from gas filamentation of femtosecond laser pulses with different durations *Opt. Express* **17** 13841
[24] Perelomov A M, Popov V S and Terent'ev M V 1966 Ionization of atoms in an alternating electric field *Sov. Phys.—JETP* **23** 924–34
[25] Dalgarno A and Kingston A E 1960 The refractive indices and Verdet constants of the inert gases *Proc. R. Soc.* A **259** 424
[26] Shelton D P 1990 Nonlinear-optical susceptibilities of gases measured at 1064 and 1319 nm *Phys. Rev.* A **42** 2578
[27] Agrawal G P 2001 *Nonlinear Fiber Optics* 3rd edn (San Diego, CA: Academic)
[28] Brée C, Demircan A, Skupin S, Bergé L and Steinmeyer G 2009 Self-pinching of pulsed laser beams during filamentary propagation *Opt. Express* **17** 16429
[29] Thomson M D, Kress M, Löffler T and Roskos H 2007 Broadband THz emission from gas plasmas induced by femtosecond optical pulses from fundamentals to applications *Laser Photon. Rev.* **1** 349